Simulations of dipolar fluids using effective many-body isotropic interactions

Simulations of dipolar fluids using effective many-body isotropic interactions

Julien O. Sindt[1] and Philip J. Camp[1, a)]

School of Chemistry, University of Edinburgh, David Brewster Road, Edinburgh EH9 3FJ, Scotland

(Dated: 18 September 2015)

The partition function of a system with pairwise-additive anisotropic dipole-dipole interactions is equal to that of a hypothetical system with many-body isotropic interactions [G. Stell, *Phys. Rev. Lett.* **32**, 286 (1974)]. The effective many-body interactions contain n-body contributions of all orders. Each contribution is known as an expansion in terms of the particle-particle distances r, and the coefficients are temperature dependent. The leading-order two-body term is the familiar $-r^{-6}$ attraction, and the leading-order three-body term is equivalent to the Axilrod-Teller interaction. In this work, a fluid of particles with the leading-order two-body and three-body interactions is compared to an equivalent dipolar soft-sphere fluid. Molecular simulations are used to determine the conditions under which the effective many-body interactions reproduce the fluid-phase structures of the dipolar system. The effective many-body interaction works well at moderately high temperatures, but fails at low temperatures where particle chaining is expected to occur. It is shown that an adjustment of the coefficients of the two-body and three-body terms leads to a good description of the structure of the dipolar fluid even in the chaining regime, due primarily to the ground-state linear configuration of the three-body Axilrod-Teller interaction. The vapor-liquid phase diagrams of systems with different Axilrod-Teller contributions are determined. As the strength of the three-body interaction is increased, the critical temperature and density both decrease, and disappear completely above a threshold strength, where chaining eventually suppresses the condensation transition.

[a)]Corresponding author: philip.camp@ed.ac.uk

I. INTRODUCTION

Strong dipolar interactions are important for soft-matter systems such as ferrofluids (colloidal suspensions of magnetized nanoparticles),[1–3] liquid crystals,[4] fluids of highly polar small molecules,[5] and biological molecules.[6] One of the most important characteristics of the anisotropic dipolar interaction is that the ground-state configuration is a nose-to-tail, parallel arrangement of the dipoles. This stabilizes structures where the particles form chains,[7,8] rings,[9] branched networks,[10,11] and large polarized domains.[8,12–18] Of particular note is that the formation of chains and rings has a strong effect on the phase diagram:[19,20] the vapor-liquid phase transition either disappears completely[9,21,22] or it is driven by a phase separation of different defects (chain ends and branching points).[10] What is clear is that the thermodynamic driving forces for phase separation are small in strongly dipolar fluids, and that the transition can be sustained by the addition of non-dipolar interactions.[19,23–25]

In the 1970s, Stell presented a theoretical study of the critical behavior of dipolar fluids.[26] The argument centered on the identification of a hypothetical fluid with isotropic many-body (MB) interactions that has exactly the same partition function as a fluid with anisotropic dipolar interactions. This is achieved by integrating out the orientational degrees of freedom, giving a coarse-grained interaction free energy. The key point is that these many-body interactions are all of short range, and hence the critical behavior is expected to be Ising-like. (The differences between dipolar fluids and dipolar spin systems are not important here.[27,28]) The leading-order terms in the effective two-body and three-body interactions are known, these being the $-r^{-6}$ attraction and the Axilrod-Teller (AT) potential,[29] respectively.[26,30,31] The attractive two-body interaction led de Gennes and Pincus to predict that the phase diagram of dipolar particles is simple, with vapor, liquid, and solid phases;[32] this is not the case.[2] The coefficients of the leading-order two-body and three-body interactions are temperature dependent, being proportional to T^{-1} and T^{-2}, respectively, with these being treated as small parameters (details will be presented in Section II). The ground-state configuration of three particles interacting via the AT potential is a linear chain. Hence, as the temperature in the hypothetical fluid is lowered, chain-like ordering should develop.

The main question to be answered in this work is, to what extent can the structural properties of dipolar fluids be described by the leading-order two-body and three-body interactions? Here, structural properties mean correlation functions such as the radial distribution

function (RDF) $g(r)$ and the static structure factor $S(k)$. Many attempts have been made to determine an effective two-body potential by taking angular averages of the Boltzmann distribution.[33–40] If the RDF is available,[41] then one can seek a unique density-dependent effective pair potential[42] by using iterative Boltzmann inversion starting from the potential of mean force $-k_{\mathrm{B}}T \ln g(r)$,[43,44] or by inverting the Ornstein-Zernike equation.[45] A different approach is taken here, based on a model system with two-body $-r^{-6}$ attractions and three-body AT interactions – with the aforementioned temperature-dependent coefficients – complemented by a soft-sphere repulsion. This is a simple system that should behave like a simple fluid at high temperature (where the two-body interaction dominates) and exhibit particle chaining at low temperature (where the three-body interaction dominates). The model is chosen such that it corresponds to the Lennard-Jones (LJ) fluid with additional temperature-dependent three-body AT interactions, and that it maps on to a fluid of dipolar soft spheres (DSSs). A LJ+AT model is often used to describe noble-gas fluids, where the coefficient of the AT interaction (ν) is related to the atomic polarizability.[46–50] In noble-gas fluids, the three-body interaction makes a relatively small contribution to the total energy ($\nu/\varepsilon\sigma^9 \sim 0.1$ where ε and σ are the LJ energy and range parameters, respectively) and ν is practically independent of temperature. In the model studied here, the strengths of the two-body and three-body interactions are strongly temperature dependent, and, as indicated above, this should give rise to chain formation at low temperature. One aim of this work is to show whether the isotropic many-body interaction can act as a proxy for the anisotropic dipolar interaction; this is achieved by determining fluid-phase structures using Monte Carlo (MC) and molecular dynamics (MD) simulations. Although not studied here, there could be some computational benefit in describing dipolar fluids with short-range many-body interactions: summing over triples of particles is expensive, but it can be done efficiently with neighbor or cell lists.[51,52] In some circumstances, this might prove preferable to techniques such as Ewald summations. Another aim of this work is to explore the effect of particle chaining – caused by an AT interaction of variable strength – on the vapor-liquid phase transition. Coexistence envelopes are computed using grand-canonical MC simulations, in combination with multicanonical sampling and histogram reweighting techniques.

The rest of this article is organized as follows. In Section II, the many-body interactions will be defined and incorporated in to a simple model that interpolates between a LJ fluid and the DSS fluid. Simulation techniques are detailed in Section III. Section IV contains

the results, and is focused on a comparison of fluid-phase structural correlation functions in the effective many-body system and the DSS fluid, and then on the vapor-liquid coexistence envelopes with different three-body interaction strengths. Section V concludes the article.

II. MODELS

A. Effective many-body interactions

It has been shown that the partition function for a system of N particles interacting via the two-body anisotropic dipole-dipole interaction

$$u_{\rm D}(\boldsymbol{r}_i, \boldsymbol{r}_j, \boldsymbol{\mu}_i, \boldsymbol{\mu}_j) = \frac{(\boldsymbol{\mu}_i \cdot \boldsymbol{\mu}_j)}{r_{ij}^3} - \frac{3(\boldsymbol{\mu}_i \cdot \boldsymbol{r}_{ij})(\boldsymbol{\mu}_j \cdot \boldsymbol{r}_{ij})}{r_{ij}^5} \tag{1}$$

is equal to that for a hypothetical fluid with isotropic many-body interactions.[26] Here, $\boldsymbol{\mu}_i$ is the dipole moment on particle i, $\boldsymbol{r}_{ij} = \boldsymbol{r}_j - \boldsymbol{r}_i$ is the interparticle separation vector, and $r_{ij} = |\boldsymbol{r}_{ij}|$. The many-body interactions arise from integrating out the dipolar orientations at inverse temperature $\beta = 1/k_{\rm B}T$. The interaction free energy of the hypothetical system is given by

$$\Psi = \sum_{i<j}^{N} \psi_2(\boldsymbol{r}_i, \boldsymbol{r}_j) + \sum_{i<j<k}^{N} \psi_3(\boldsymbol{r}_i, \boldsymbol{r}_j, \boldsymbol{r}_k) + \ldots \tag{2}$$

These are free energies because they contain entropic contributions from integrating out the orientational degrees of freedom. For a one-component fluid in which $\mu = |\boldsymbol{\mu}|$ for each particle, the leading-order terms in the two-body and three-body interactions are[26,30,31]

$$\beta\psi_2(\boldsymbol{r}_i, \boldsymbol{r}_j) = -\frac{(\beta\mu^2)^2}{3r_{ij}^6} \tag{3}$$

$$\beta\psi_3(\boldsymbol{r}_i, \boldsymbol{r}_j, \boldsymbol{r}_k) = \frac{(\beta\mu^2)^3}{9} \frac{(1 + 3\cos\alpha_i \cos\alpha_j \cos\alpha_k)}{r_{ij}^3 r_{jk}^3 r_{ik}^3} \tag{4}$$

where α_i, α_j, and α_k are the interior angles of the triangle formed by particles i, j, and k. Equation (4) is equivalent to the AT potential with a temperature-dependent strength.[29] Note that the higher order terms in ψ_2 and ψ_3 are of shorter range, and at least in the case of the two-body potential, easy to evaluate.[35,40] They are omitted here for two reasons: firstly, the complete pair-potential of mean force (w_2) would not be accurate in the regime where a high degree of chaining of the particles is expected; secondly, the aim is to study a simple interaction potential with a small number of coefficients, and with a well-known limit (the LJ potential, as shown below).

Introducing the particle diameter σ, the dimensionless dipolar coupling constant is defined as $\lambda = \mu^2/k_{\rm B}T\sigma^3$. Equations (3) and (4) can then be rewritten in the form

$$\beta\psi_2(\boldsymbol{r}_i, \boldsymbol{r}_j) = -\frac{\lambda^2}{3}\left(\frac{\sigma}{r_{ij}}\right)^6 \tag{5}$$

$$\beta\psi_3(\boldsymbol{r}_i, \boldsymbol{r}_j, \boldsymbol{r}_k) = \frac{\lambda^3}{9} f_3(\boldsymbol{r}_i, \boldsymbol{r}_j \boldsymbol{r}_k) \tag{6}$$

$$f_3(\boldsymbol{r}_i, \boldsymbol{r}_j \boldsymbol{r}_k) = (1 + 3\cos\alpha_i \cos\alpha_j \cos\alpha_j)\left(\frac{\sigma^9}{r_{ij}^3 r_{jk}^3 r_{ik}^3}\right). \tag{7}$$

The many-body interactions are determined by expanding out the partition functions of the original and hypothetical systems in terms of λ, and then matching terms involving equal numbers of particles.

This system can be mapped on to a system of LJ particles with an additional three-body AT interaction as follows. Firstly, add a short-range, soft-sphere repulsion $(4/T^*)(\sigma/r_{ij})^{12}$ to complement Eq. (5), where $T^* = k_{\rm B}T/\varepsilon$, and ε is the LJ energy parameter. Secondly, make the short-range repulsion and two-body attraction (5) add up to the Lennard-Jones potential by fixing $4/T^* = \lambda^2/3$. Finally, express the prefactor of the three-body interaction in Eq. (6) as $\lambda^3/9 = (a/T^*)^{3/2}$ where $a = 4/\sqrt[3]{3} \simeq 2.77$; this special value of a will hereafter be denoted by $a_{\rm D}$. The two-body interaction w_2 and the three-body interaction w_3 (in units of $k_{\rm B}T$) are then given by

$$\beta w_2(\boldsymbol{r}_i, \boldsymbol{r}_j) = \frac{4}{T^*}\left[\left(\frac{\sigma}{r_{ij}}\right)^{12} - \left(\frac{\sigma}{r_{ij}}\right)^6\right] \tag{8}$$

$$\beta w_3(\boldsymbol{r}_i, \boldsymbol{r}_j, \boldsymbol{r}_k) = \left(\frac{a}{T^*}\right)^{3/2} f_3(\boldsymbol{r}_i, \boldsymbol{r}_j, \boldsymbol{r}_k) \tag{9}$$

and the total interaction free energy W is defined by

$$\beta W = \sum_{i<j} \beta w_2(\boldsymbol{r}_i, \boldsymbol{r}_j) + \sum_{i<j<k} \beta w_3(\boldsymbol{r}_i, \boldsymbol{r}_j, \boldsymbol{r}_k). \tag{10}$$

It is convenient to refer to this as the effective many-body (EMB) potential, although the unusual temperature dependence of w_3 reminds us that it is the statistical free energy of interaction, and not the mechanical potential energy.[53] A family of EMB potentials can be generated by treating a as an adjustable parameter: $a = 0$ corresponds to the LJ potential; and the dipolar limit corresponds to $a = a_{\rm D}$.

To get an idea of the EMB free-energy surface, Figure 1 shows plots of the two-body, three-body, and total contributions for three particles in a plane, with separations $r_{12} = r_{13} = 2^{1/6}\sigma$

(the position of the minimum in the LJ potential), and angle θ given by $(\boldsymbol{r}_{12} \cdot \boldsymbol{r}_{13}) = r_{12} r_{13} \cos\theta$. $\theta = \pi$ corresponds to a linear chain, while $\theta = \pi/3$ and $5\pi/3$ correspond to an equilateral triangle. The interaction free energies are given by

$$W_2 = w_2(\boldsymbol{r}_1, \boldsymbol{r}_2) + w_2(\boldsymbol{r}_2, \boldsymbol{r}_3) + w_2(\boldsymbol{r}_1, \boldsymbol{r}_3), \tag{11}$$

$$W_3 = w_3(\boldsymbol{r}_1, \boldsymbol{r}_2, \boldsymbol{r}_3), \tag{12}$$

$$W_{\text{total}} = W_2 + W_3 \tag{13}$$

where the Boltzmann probability of observing a particular cluster is proportional to $\exp(-\beta W_{\text{total}})$.[53] Figure 1(a) shows W_2, W_3, and W_{total} with $a = a_{\text{D}}$ and $T^* = 3.0$; recall that the relative contributions from w_2 and w_3 depend on temperature. W_2 favors the compact cluster and W_3 favors the linear chain; at $T^* = 3.0$, the latter dictates the ground-state configuration. Figure 1(b) shows W_{total} at three temperatures, $T^* = 0.1$, 1.0, and 3.0. As the temperature is reduced, the three-body AT interaction becomes more dominant, and the linear-chain configuration becomes increasingly favored over compact configurations.

B. Dipolar soft spheres

The pair potential in the dipolar soft-sphere (DSS) model is

$$u_{\text{DSS}}(\boldsymbol{r}_i, \boldsymbol{r}_j, \boldsymbol{\mu}_i, \boldsymbol{\mu}_j) = 4\varepsilon \left(\frac{\sigma}{r}\right)^{12} + u_{\text{D}}(\boldsymbol{r}_i, \boldsymbol{r}_j, \boldsymbol{\mu}_i, \boldsymbol{\mu}_j). \tag{14}$$

Replacing the dipolar interaction u_{D} with its many-body counterpart, and setting $T^* = 12/\lambda^2$ as in Section II A, gives the two-body and three-body effective potentials in Eqs. (8) and (9), respectively. Hence, there is a direct correspondence between the EMB and DSS fluids.

Of particular interest in dipolar fluids is the formation of chains. Roughly speaking, chaining occurs when the thermal energy is about one-quarter of the dipole-dipole interaction energy, i.e., $\lambda > 4$.[7] For dipolar hard spheres, the definition of the dipolar coupling constant is unambiguous, because the distance of closest approach of two particles is precisely equal to the sphere diameter d, the minimum pair energy $u_0 = -2\mu^2/d^3$, and the dipolar coupling constant $\lambda = -u_0/2k_{\text{B}}T$. The effective dipolar coupling constant in the DSS fluid is, however, less than the parameter $\lambda = \mu^2/k_{\text{B}}T\sigma^3$ because the lowest-energy distance between a pair of particles is greater than σ due to the soft-sphere repulsion. Two ways of correcting for this

are the Barker-Henderson scheme[54,55] and a method based on the minimum of the dipolar pair potential. In the Barker-Henderson scheme, the effective hard-sphere diameter d for the soft-sphere repulsion $4\varepsilon(\sigma/r)^{12}$ is

$$d = \sigma \left(\frac{4}{T^*}\right)^{1/12} \Gamma\left(\frac{11}{12}\right). \tag{15}$$

The effective dipolar coupling constant is therefore given by

$$\lambda_{\text{eff}} = \frac{\mu^2}{k_{\text{B}} T d^3} = \lambda \left(\frac{\sigma}{d}\right)^3. \tag{16}$$

Alternatively, the minimum u_0 in the pair potential can be associated with the nose-to-tail, parallel ($\rightarrow\rightarrow$) arrangement of dipolar hard spheres. The ground-state energy of a pair of DSSs is

$$\frac{u_0}{k_{\text{B}} T} = \frac{4}{T^*} \left(\frac{\sigma}{r_0}\right)^{12} - 2\lambda \left(\frac{\sigma}{r_0}\right)^3 = -\frac{3}{4} \lambda^{4/3} (T^*)^{1/3} \tag{17}$$

with

$$r_0 = \sigma \left(\frac{8}{\lambda T^*}\right)^{1/9}. \tag{18}$$

This leads to the result

$$\lambda_{\text{eff}} = -\frac{u_0}{2 k_{\text{B}} T} = \frac{3}{8} \lambda^{4/3} (T^*)^{1/3}. \tag{19}$$

The two formulations of the effective dipolar coupling constant are compared in Fig. 2 as a function of $\lambda = \sqrt{12/T^*}$. The key point is that to achieve $\lambda_{\text{eff}} \simeq 4$, where chaining is anticipated, λ should be approximately 10–15.

C. Thermodynamics

The EMB interaction free energy $W(\beta)$ is determined by the condition that the configurational integral (partition function) Z of the hypothetical fluid is equal to that of the original fluid at any given temperature. The thermodynamic relation between the configurational part of the internal energy E, and the corresponding Helmholtz free energy $F = -k_{\text{B}} T \ln Z$, is $E = (\partial \beta F / \partial \beta)_{N,V}$. For a system in which the effective interaction energy $W(\beta)$ is a function of β, Z and E are given by[53]

$$Z = \int \mathrm{d}\boldsymbol{r}_1 \ldots \int \mathrm{d}\boldsymbol{r}_N \exp\left(-\beta W\right) \tag{20}$$

$$E = \left\langle \frac{\partial(\beta W)}{\partial \beta} \right\rangle_{N,V}. \tag{21}$$

Note that for the DSS system with λ slaved to β by the relation $\lambda = \sqrt{12\beta\epsilon}$, $u_{\rm DSS}$ is effectively temperature dependent, and should formally be viewed as a free energy. The relationship for E given above is therefore appropriate in this case. In coarse-graining approaches, the resulting interaction free energy can depend not only on temperature, but also on density. There are well-known and serious problems of thermodynamic consistency with density-dependent 'potentials',[56] but the effective potential derived here depends only on temperature, and so these problems do not have to be considered here.

III. SIMULATIONS

In all cases, simulations were carried out in a cubic box of volume $V = L^3$, and with periodic boundary conditions applied. The DSS system was studied with NVT MD simulations, carried out using LAMMPS.[57,58] The long-range dipolar interaction was handled with an Ewald summation and conducting boundary conditions. Structural properties were determined with systems of $N = 512$ particles at three reduced densities, $\rho^* = \rho\sigma^3 = 0.007$, 0.100, and 0.450, where $\rho = N/V$. With strongly interacting dipolar particles, these densities are known to be representative of chained, network, and 'normal' fluid states.[59,60] Temperatures $T^* = 12/\lambda^2$ were selected corresponding to dipolar coupling constants in the range $1 \leq \lambda \leq 20$ ($12.0 \geq T^* \geq 0.0300$).

The properties of the EMB system were studied using NVT MC simulations according to the appropriate Boltzmann probability proportional to $\exp(-\beta W)$.[53] The system sizes and box dimensions were exactly the same as in the MD simulations of DSSs. The two-body LJ interactions were truncated at $L/2$. The three-body AT interactions were evaluated using the minimum-image convention outlined by Attard,[46] which removes any ambiguities in identifying triples of particles: effectively, the potential is truncated if the distance between any two particles in a triplet is greater than $L/2$. The MC code was tested carefully against the simulation data for a fluid with LJ and AT interactions presented in Ref. 46.

The vapor-liquid coexistence envelope of the EMB system (with variable AT-interaction strength a) was determined using μVT grand-canonical Monte Carlo (GCMC) simulations, with multicanonical biasing in the particle number N to enforce proper sampling of the coexisting phases.[61] The box lengths were fixed in the range $7 \leq L/\sigma \leq 12$, depending on the system parameters and whether significant particle chaining warranted a bigger box.

In these calculations, the LJ potential was truncated and shifted at $r_c = 2.5\sigma$. From a mixed-field finite-size scaling analysis,[62] the critical parameters of the corresponding LJ system (i.e., with $a = 0$) are $T_c^* = 1.0795(2)$ and $\rho_c^* = 0.3211(5)$.[63] In this work, the conditions for phase coexistence at fixed T were estimated by tuning the chemical potential at fixed T with histogram reweighting to yield a bimodal particle-number distribution with equal peak areas.[61] The average particle numbers, and hence densities, for the peaks were then calculated to yield the coexistence densities ρ_- (vapor) and ρ_+ (liquid). The critical parameters were estimated from $\rho_\pm(T < T_c)$ by using the order-parameter scaling law and law of rectilinear diameters given by

$$\frac{1}{2}(\rho_+ - \rho_-) = Bt^\beta \tag{22}$$

$$\frac{1}{2}(\rho_+ + \rho_-) = \rho_c + At \tag{23}$$

where $t = 1 - T/T_c$, $\beta = 0.326$ is the Ising order-parameter exponent, and A and B are non-universal coefficients. A mixed-field finite-size scaling analysis has not been carried out due to the large computational effort required for the many-body interactions.

IV. RESULTS

In Section IV A the structures and internal energies of the DSS fluid will be compared with those of the EMB fluid with $a = a_D$, i.e., with the three-body AT interaction strength as determined by theory.[26,30,31] In Section IV B the EMB parameters will be varied independently to reproduce the highly chained structures seen in DSS fluids with large values of λ. In Section IV C, the vapor-liquid coexistence curves will be presented for EMB systems with various values of a.[64]

A. Fluid structures and internal energies of DSSs and EMB particles with $a = a_D$

Figure 3 shows simulation snapshots of DSS and EMB fluids at $\rho^* = 0.007$, and with $\lambda = 1$–20. With $\lambda = 1$ and 2, both systems look like a regular dilute gas. At $\lambda = 5$, there are some small clusters in both the DSS and EMB systems. With $\lambda = 10$, there are some moderately sized, chain-like clusters in the DSS fluid, while the EMB fluid is almost

entirely aggregated in to linear chains, with a small number of branching points. At the extreme value of $\lambda = 20$, both the DSS and EMB systems are fully clustered, but the chains in the EMB system are clearly much more linear and rigid. These observations give the first indication of the regime in which the EMB potential might mimic the DSS potential. As explained in Section II A, the many-body interactions are determined by expanding the partition function in terms of the parameter λ. Only the leading-order contributions to the two-body and three-body interactions have been retained, and all higher order contributions have been omitted. As λ is increased, and T^* is reduced, the three-body term becomes dominant, without any compensation from higher order terms. Hence, chain formation simply becomes strongly favored. Ring formation is important in dictating the thermodynamics and magnetic properties of dipolar systems at very low densities and very low temperatures.[9,22,65] Transient rings are observed to coexist with chains in the DSS system at $\rho^* = 0.007$ and $\lambda = 20$ ($\lambda_{\rm eff} \simeq 5$–$6$). Under these conditions the structure of the EMB system is dominated by rigid chains. More terms would have to be added to the EMB interaction in order to mimic the DSS system. It is possible that rings exist in the current EMB system at much lower densities, but this has not been explored here.

Figure 4 shows the RDFs of the DSS and EMB fluids at $\rho^* = 0.007$, 0.100, and 0.450, and with $\lambda = 1$–20. For a given concentration, the RDFs of the DSS and EMB fluids are practically identical with $\lambda = 1$ and 2. With $\lambda = 5$, and at $\rho^* = 0.007$ and 0.100, the structure in the EMB fluid is more pronounced, but the primary peak position is unchanged at $r \simeq \sigma$; at $\rho^* = 0.450$, the DSS fluid shows more structure. With $\lambda = 10$ and 20, and at all concentrations, the RDFs of the EMB fluid show much sharper peaks shifted to shorter distances than those of the DSS fluid. This reflects the crossover to very pronounced chaining in the EMB, evident in the snapshots. The RDF of the DSS fluid with $\lambda = 20$ and at $\rho^* = 0.450$ shows that the system has crystallized. Although the density appears to be quite low, the effective density is $\rho R^3 \simeq 1.34$, where $R \simeq 1.44\sigma$ is the nearest-neighbor distance as determined from the RDF.

Figure 5 shows the static structure factors, $S(k)$, for the DSS and EMB fluids at the same state points. $S(k)$ was calculated directly from the formula

$$S(\boldsymbol{k}) = \frac{1}{N}\langle \rho(\boldsymbol{k})\rho(-\boldsymbol{k})\rangle \tag{24}$$

where $\boldsymbol{k} = (2\pi/L)(n_x, n_y, n_z)$ ($n_x, n_y, n_z = 0, \pm 1, \pm 2, \ldots$) is a wavevector commensurate with

the periodic boundary conditions, and $\rho(\boldsymbol{k}) = \sum_{j=1}^{N} \exp\left(-\mathrm{i}\boldsymbol{k}\cdot\boldsymbol{r}_j\right)$ is a Fourier component of the density. The results are averaged over wavevectors of equal magnitude $k = |\boldsymbol{k}|$. The results in Fig. 5 mirror those in Fig. 4. At all densities, the results with $\lambda = 1$ and 2 are the same in both the DSS and EMB fluids. With $\lambda = 5$, the peak positions match up, but the degrees of ordering reflected in the peak heights are different. With $\lambda = 10$ and 20, the results are fundamentally different. $S(k)$ for the DSS fluid with $\lambda = 20$ and $\rho^* = 0.450$ shows Bragg peaks, signaling crystallization. In both the DSS and EMB fluids with $\lambda = 10$ and 20, and at $\rho^* = 0.007$, the low-k behavior of the static structure factor shows a k^{-1} 'divergence' characteristic of chaining.[60] This will be discussed further in the next section.

One signature of particle association – particularly at low concentrations – is a rapid drop in internal energy with decreasing temperature, and an associated peak in the heat capacity. Figure 6 shows the configurational part of the internal energy of DSSs at $\rho^* = 0.007$, as a function of $\beta^* = 1/T^*$. As a result of fixing $\lambda = \sqrt{12/T^*}$, u_{DSS} [Eq. (14)] is temperature dependent, and hence should be formally viewed as a free energy. The internal energy defined in Eq. (21) is therefore given by

$$\frac{\beta E}{N} = \frac{1}{N}\left\langle \sum_{i<j}\left[\frac{4}{T^*}\left(\frac{\sigma}{r_{ij}}\right)^{12} + \frac{1}{2}\beta u_{\mathrm{D}}(\boldsymbol{r}_i, \boldsymbol{r}_j, \boldsymbol{\mu}_i, \boldsymbol{\mu}_j)\right]\right\rangle \tag{25}$$

The MD simulation results show that the energy first drops with decreasing temperature to a minimum, and then slowly increases again. Fitting the simulation data with [2/2] Padé approximant in β^* (as shown in Fig. 6) and differentiating gives the constant-volume heat capacity $C_V = -k_{\mathrm{B}}\beta^2(\partial E/\partial\beta)_{N,V}$, which shows a primary peak at $\beta^* \simeq 11.1$, corresponding to $\lambda \simeq 11.5$. This peak corresponds to the onset of chaining, and its position corresponds closely to the range predicted in Section II B. The behavior at very low temperature (high β^*) can be understood as follows. In the chaining regime, almost every particle will have two nearest neighbors in the nose-to-tail, parallel conformation ($\rightarrow\rightarrow$). At low temperatures, the most probable nearest-neighbor distance will then be close to r_0, defined in Eq. (18). Hence, the most probable internal energy will be given by the two terms in the angled brackets in Eq. (25). This gives the following explicit results for the total internal energy E, and the soft-sphere and dipolar contributions E_{SS} and E_{D}, respectively.

$$\frac{E}{N\varepsilon} = -\left(\frac{3}{2\beta^*}\right)^{2/3} \tag{26}$$

$$\frac{E_{\mathrm{SS}}}{N\varepsilon} = \left(\frac{3}{2\beta^*}\right)^{2/3} \tag{27}$$

$$\frac{E_{\mathrm{D}}}{N\varepsilon} = -2\left(\frac{3}{2\beta^*}\right)^{2/3} \tag{28}$$

These curves are included in Fig. 6. Good agreement is found with the simulation results for $\beta^* \gtrsim 25$ (or $\lambda \gtrsim 17$), and this is firmly in the chaining regime. Finally, the internal energy of the EMB system coincides with the DSS energy only with $\beta \lesssim 1$ or $\lambda \lesssim 3$. Beyond this value, the three-body term becomes dominant, leading to a rapid decrease in energy, and the deviations in structure detailed above.

B. Fluid structures of DSSs and EMB particles with other potential parameters

In the previous section, it was shown that the structures of the DSS and EMB fluids are only equal with $\lambda \sim 1$, although this is a typical value of the dipolar coupling constant in a real ferrofluid.[1] In this section, the focus will be on whether the chain-like structures of the DSS fluid at low concentrations and low temperature can be mimicked with an EMB potential by tuning the various parameters independently. The DSS fluid has been considered at $\rho^* = 0.007$ and 0.100, and with $\lambda = 15$ ($T^* = 12/\lambda^2 = 0.0533$); $\rho^* = 0.450$ was omitted due to the possibility of solid formation. The RDFs and static structure factors were compared to those for an EMB system with the following interactions.

$$\beta w_2(\boldsymbol{r}_i, \boldsymbol{r}_j) = \frac{4}{T^*}\left(\frac{\bar{\varepsilon}}{\varepsilon}\right)\left[\left(\frac{\bar{\sigma}}{r_{ij}}\right)^{12} - \left(\frac{\bar{\sigma}}{r_{ij}}\right)^{6}\right] \tag{29}$$

$$\beta w_3(\boldsymbol{r}_i, \boldsymbol{r}_j, \boldsymbol{r}_k) = \left(\frac{a}{T^*}\right)^{3/2}\left(\frac{\bar{\sigma}}{\sigma}\right)^{9} f_3(\boldsymbol{r}_i, \boldsymbol{r}_j, \boldsymbol{r}_k) \tag{30}$$

$\bar{\varepsilon}$ and $\bar{\sigma}$ are effective LJ energy and range parameters, respectively, and the AT interaction parameter a is also adjustable. Mappings between the DSS and EMB potentials were sought, based on attempts to match or align the energy surfaces of clusters of three particles, or infinite chains of particles, but none was successful. So instead, $\bar{\varepsilon}$, $\bar{\sigma}$, and a were adjusted heuristically until a reasonable match was obtained between the structures of the DSS and EMB fluids. Note that the EMB fluid was simulated at the same *reduced* density $\rho\bar{\sigma}^3 = \rho^*$, so that $\bar{\sigma}$ simply represents a change of scale.

Figure 7 shows the results for the DSS fluid, the EMB fluid with the original parameters ($\bar{\varepsilon} = \varepsilon$, $\bar{\sigma} = \sigma$, $a = a_{\mathrm{D}}$), and the EMB fluid with parameters that have been tuned to give a reasonable match with the DSS fluid. Figure 7(a)–(c) shows the results for $\rho^* = 0.007$. In this case, the matched EMB fluid has parameters $\bar{\varepsilon} = 0.25\varepsilon$, $\bar{\sigma} = 1.20\sigma$, and $a = 0.42$. The RDF of the DSS fluid shows the strong, localized peaks characteristic of chain-like structures. A snapshot of the fluid is shown in Fig. 8. The RDF of the original EMB fluid shows too much structure, and the peaks are shifted to shorter distances, reflecting an effective particle size that is too small. The snapshot in Fig. 8 shows that the chains are too rigid, and that there are no dissociated particles. The RDF of the matched EMB fluid has peaks in the correct places and of the correct heights, and the snapshot in Fig. 8 looks much closer to that of the DSS fluid: there is a mixture of chains and free particles, and the chains are not too rigid. The static structure factors shown in Fig. 7(b) show the same thing: the matched EMB fluid is a reasonable mimic of the DSS fluid. A log-log plot of $S(k)$ in Fig. 7(c) confirms the k^{-1} behavior expected for chain-like structures.[60]

Figure 7(d)–(f) shows the results for $\rho^* = 0.100$. The matched EMB fluid has parameters $\bar{\varepsilon} = 0.19\varepsilon$, $\bar{\sigma} = 1.16\sigma$, and $a = 0.37$. As before, the structure in the original EMB fluid is too pronounced, and the effective particle diameter is too small. The matched EMB fluid exhibits structures on the right lengthscales, and of similar degrees to those in the DSS fluid. The snapshots in Fig. 8 confirm these statements, with strong chaining being apparent in the original EMB system even at this moderate concentration.

Overall, the agreement between the structures of the DSS fluid and the matched EMB fluid is not perfect, but one would not expect them to be, as it is not possible to fit the energy surface of the dipolar system with a simple truncated form for the effective-potential function. Nonetheless, the results show that similar structures can be observed in the DSS and EMB systems.

C. Phase separation of the EMB fluid with variable a

Particle aggregation in dipolar fluids at low temperatures is thought to interrupt vapor-liquid phase separation.[9,21,22] In the EMB model, this can be studied directly by tuning the AT interaction parameter a: when $a = 0$, the EMB potential is equivalent to the LJ potential, for which the critical properties are known precisely. Just to reiterate, the LJ part

of the EMB potential is truncated and shifted at $r_c = 2.5\sigma$, and for this system, the critical parameters are $T_c^* = 1.0795(2)$ and $\rho_c = 0.3211(5)$.[63] The aim here is to study EMB systems with $a \geq 0$, and to determine the effects of particle chaining on the phase transition. Systems have been studied with $a^{3/2} = 0$, 0.1, 0.2, 0.5, 0.75, and 1. The vapor-liquid coexistence envelopes are shown in Fig. 9(a), as determined from GCMC simulations, and as fitted using the scaling laws in Eqs. (22) and (23). The first point is that the simulation results are fitted extremely well by the scaling laws; the critical parameters extracted from the fits are given in Table I. Secondly, the critical parameters for the system with $a = 0$ are in excellent agreement with published data for the LJ system.[63] Thirdly, the critical temperature, the critical density, and the width of the coexistence envelope decrease with increasing a; this is reminiscent of the trends seen in patchy colloids, as the valence of the particles is reduced.[66] Figure 9(b) shows plots of the critical parameters versus $a^{3/2}$. It appears that they decrease linearly with this prefactor in the three-body interaction [Eq. (9)]. The sampling becomes difficult at low temperatures and with high values of a due to cluster formation, but linear fits to the results indicate that the transition disappears completely with $a^{3/2} = 1.5$–1.7 ($a = 1.3$–1.4). Of course, some other functional dependence on $a > 1.0$ cannot be ruled out.

The structures of the coexisting vapor and liquid phases are detailed in Figs. 10 and 11. Figure 10 shows simulation snapshots of the coexisting phases in EMB systems with $a = 0.0$ (the LJ fluid) and $a = 1.0$ and at temperatures $T < T_c$. The structure of the liquid phase is unremarkable, and does not depend strongly on the strength of the AT interactions. The vapor phase shows some clustering with $a = 1.0$ which is obviously absent with $a = 0.0$. This is shown more clearly by the vapor-phase RDFs in Fig. 11(a): with $a = 1.0$, the intense primary peak, secondary peak, and gradual decay to $g(r) = 1$ at large r are all characteristic of chain-like correlations. The liquid-phase RDFs in Fig. 11(b) are quite similar.

V. CONCLUSIONS

The structural properties and phase diagrams of a system with isotropic many-body interactions have been studied using molecular simulations. The two-body and three-body interaction free energies were determined long ago by mapping on to the partition function of a system with anisotropic dipolar interactions.[26,30,31] Only the leading-order terms in these interactions were retained, corresponding to the familiar two-body dispersion and three-body

Axilrod-Teller potentials but with temperature-dependent coefficients. These interactions were complemented by a short-range two-body repulsion. At low temperatures, the effective Axilrod-Teller interaction becomes dominant due to its temperature-dependent coefficient, resulting in chain-like ground-state structures.

At low temperatures and low concentrations, dipolar particles are known to form chain-like aggregates. The structures in the system with many-body interactions are the same as those in dipolar fluids at high temperatures, but at low temperatures, the many-body interactions overemphasize chain formation. Adjustment of the potential parameters resulted in good structural matches with dipolar fluids at low temperatures and low concentrations.

Finally, the vapor-liquid phase transition of the many-body system was tracked as a function of the strength of the three-body Axilrod-Teller interaction. As the strength of this interaction is increased, the critical temperature, critical density, and width of the coexistence envelope all decrease, and ultimately the transition disappears. This is directly linked to chain formation: as chain formation develops, the valence of the particles decreases, and the densities of the coexisting phases drop sharply.

It might be useful to develop isotropic many-body interaction potentials further as a proxy for the anisotropic dipolar interaction, and indeed as a model for chain-forming systems in general.[11,67] From a computational point of view, short-range many-body interactions could be easier to treat than long-range two-body interactions, in some situations. To this end, the two-body interaction potential can be developed in a number of ways beyond the leading-order term used in this work,[33–40,45] and the three-body Axilrod-Teller potential can be retained as the chain-forming interaction. The prospect of moving to four-body interactions is not appealing. Whether there is a computational benefit of using many-body interactions or not, the model studied in this work has yielded some direct insights on the effects of chain-stabilizing interactions on fluid structure and phase separation.

ACKNOWLEDGMENTS

This research was supported by the Engineering and Physical Sciences Research Council through the provision of a studentship to J.O.S.

REFERENCES

[1]R. E. Rosensweig, *Ferrohydrodynamics* (Dover Publications, Inc., New York, 1998).

[2]P. I. C. Teixeira, J. M. Tavares, and M. M. Telo da Gama, J. Phys.: Condens. Matter **12**, R411 (2000).

[3]C. Holm and J.-J. Weis, Curr. Opin. Colloid Interface Sci. **10**, 133 (2005).

[4]R. B. Meyer, L. Liebert, L. Strzelecki, and P. Keller, J. Phys. Lett. (Paris) **36**, L69 (1975).

[5]M. A. Suhm, Ber. Bunsenges. phys. Chem. **99**, 1159 (1995).

[6]C. Branden and J. Tooze, *Introduction to Protein Structure*, 2nd ed. (Garland Publishing, Inc., New York, 1998).

[7]J. J. Weis and D. Levesque, Phys. Rev. Lett. **71**, 2729 (1993).

[8]D. Levesque and J. J. Weis, Phys. Rev. E **49**, 5131 (1994).

[9]L. Rovigatti, J. Russo, and F. Sciortino, Soft Matter **8**, 6310 (2012).

[10]T. Tlusty and S. A. Safran, Science **290**, 1328 (2000).

[11]A. Zilman, T. Tlusty, and S. A. Safran, J. Phys.: Condens. Matter **15**, S57 (2003).

[12]R. Tao and J. M. Sun, Phys. Rev. Lett. **67**, 398 (1991).

[13]D. Wei and G. N. Patey, Phys. Rev. Lett. **68**, 2043 (1992).

[14]D. Wei and G. N. Patey, Phys. Rev. A **46**, 7783 (1992).

[15]J. J. Weis and D. Levesque, Phys. Rev. E **48**, 3728 (1993).

[16]J.-J. Weis, J. Chem. Phys. **123**, 044503 (2005).

[17]J.-J. Weis and D. Levesque, J. Chem. Phys. **125**, 034504 (2006).

[18]M. A. Pounds and P. A. Madden, J. Chem. Phys. **126**, 104506 (2007).

[19]G. Ganzenmüller, G. N. Patey, and P. J. Camp, Mol. Phys. **107**, 403 (2009).

[20]L. Rovigatti, J. M. Tavares, and F. Sciortino, Phys. Rev. Lett. **111**, 168302 (2013).

[21]M. E. van Leeuwen and B. Smit, Phys. Rev. Lett. **71**, 3991 (1993).

[22]L. Rovigatti, J. Russo, and F. Sciortino, Phys. Rev. Lett. **107**, 237801 (2011).

[23]G. Ganzenmüller and P. J. Camp, J. Chem. Phys. **126**, 191104 (2007).

[24]N. G. Almarza, E. Lomba, C. Martín, and A. Gallardo, J. Chem. Phys. **129**, 234504 (2008).

[25]S. Dussi, L. Rovigatti, and F. Sciortino, Mol. Phys. **111**, 3608 (2013).

[26]G. Stell, Phys. Rev. Lett. **32**, 286 (1974).

[27]A. Aharony and M. E. Fisher, Phys. Rev. B **8**, 3323 (1973).

[28]A. D. Bruce and A. Aharony, Phys. Rev. B **10**, 2078 (1974).

[29]B. M. Axilrod and E. Teller, J. Chem. Phys. **11**, 299 (1943).

[30]B. Linder, J. Chem. Phys. **40**, 2003 (1964).

[31]J. C. Rasaiah and G. Stell, Chem. Phys. Lett. **25**, 519 (1974).

[32]P. G. de Gennes and P. A. Pincus, Phys. Kondens. Materie **11**, 189 (1970).

[33]C. E. Woodward and S. Nordholm, Mol. Phys. **52**, 973 (1984).

[34]D. Y. C. Chan and D. Henderson, J. Colloid Interface Sci. **101**, 419 (1984).

[35]D. Y. C. Chan, D. Henderson, J. Barojas, and A. M. Homola, IBM J. Res. Develop. **29**, 11 (1985).

[36]J. M. Mercer, Mol. Phys. **69**, 625 (1990).

[37]P. Frodl and S. Dietrich, Phys. Rev. A **45**, 7330 (1992).

[38]P. Frodl and S. Dietrich, Phys. Rev. A **48**, 3203 (1993).

[39]J. M. Tavares, M. M. Telo da Gama, and M. A. Osipov, Phys. Rev. E **56**, R6252 (1997).

[40]A. P. Philipse and B. W. M. Kuipers, J. Phys.: Condens. Matter **22**, 325104 (2010).

[41]E. A. Elfimova, A. O. Ivanov, and P. J. Camp, J. Chem. Phys. **136**, 194502 (2012).

[42]R. L. Henderson, Phys. Lett. A **49**, 197198 (1974).

[43]R. L. McGreevy and L. Pusztai, Mol. Sim. **1**, 359367 (1988).

[44]A. P. Lyubartsev and A. Laaksonen, Phys. Rev. E **52**, 37303737 (1995).

[45]P. I. C. Teixeira, J. Phys.: Condens. Matter **25**, 195102 (2013).

[46]P. Attard, Phys. Rev. A **45**, 5649 (1992).

[47]R. J. Sadus and J. M. Prausnitz, J. Chem. Phys. **104**, 4784 (1996).

[48]J. A. Anta, E. Lomba, and M. Lombardero, Phys. Rev. E **55**, 2707 (1997).

[49]R. J. Sadus, Fluid Phase Equil. **144**, 351 (1998).

[50]F. Goujon, P. Malfreyt, and D. J. Tildesley, J. Chem. Phys. **140**, 244710 (2014).

[51]M. P. Allen and D. J. Tildesley, *Computer simulation of liquids* (Clarendon Press, Oxford, 1987).

[52]D. Frenkel and B. Smit, *Understanding Molecular Simulation: From Algorithms to Applications*, 2nd ed. (Academic Press, San Diego, 2001).

[53]G. S. Rushbrooke, Trans. Faraday Soc. **36**, 1055 (1940).

[54]J. A. Barker and D. Henderson, J. Chem. Phys. **47**, 4714 (1967).

[55]J.-P. Hansen and I. R. McDonald, *Theory of Simple Liquids*, 3rd ed. (Academic Press, London, 2006).

[56]A. A. Louis, J. Phys.: Condens. Matter **14**, 9187 (2002).

[57]"LAMMPS Molecular Dynamics Simulator," http://lammps.sandia.gov.

[58]S. Plimpton, J. Comp. Phys. **117**, 1 (1995).

[59]P. J. Camp, J. C. Shelley, and G. N. Patey, Phys. Rev. Lett. **84**, 115 (2000).

[60]P. J. Camp and G. N. Patey, Phys. Rev. E **62**, 5403 (2000).

[61]A. Z. Panagiotopoulos, J. Phys.: Condens. Matter **12**, R25 (2000).

[62]N. B. Wilding, Phys. Rev. E **52**, 602 (1995).

[63]W. Shi and J. K. Johnson, Fluid Phase Equil. **187-188**, 171 (2001).

[64]Original simulation data are available from http://dx.doi.org/10.7488/ds/276.

[65]S. Kantorovich, A. O. Ivanov, L. Rovigatti, J. M. Tavares, and F. Sciortino, Phys. Rev. Lett. **110**, 148306 (2013).

[66]E. Bianchi, J. Largo, P. Tartaglia, E. Zaccarelli, and F. Sciortino, Phys. Rev. Lett. **97**, 168301 (2006).

[67]J.-J. Weis and D. Levesque, Adv. Polym. Sci. **185**, 163 (2005).

TABLE I. Vapor-liquid critical parameters for the EMB system with various values of the AT interaction parameter a.

a	$a^{3/2}$	T_c^*	ρ_c^*	Source
0.000	0.000	1.0795(2)	0.3211(5)	Ref. 63
0.000	0.000	1.0789(8)	0.324(1)	This work
0.215	0.100	1.001(2)	0.3040(9)	
0.342	0.200	0.922(2)	0.284(1)	
0.630	0.500	0.702(4)	0.219(2)	
0.825	0.750	0.54(1)	0.173(5)	
1.000	1.000	0.396(4)	0.131(1)	

FIG. 1. Two-body, three-body, and total interaction free energies (W_2, W_3, and $W_{\rm total}$, respectively) for a cluster of three particles in a plane with $a = a_{\rm D}$. The energies are plotted in units of ε.

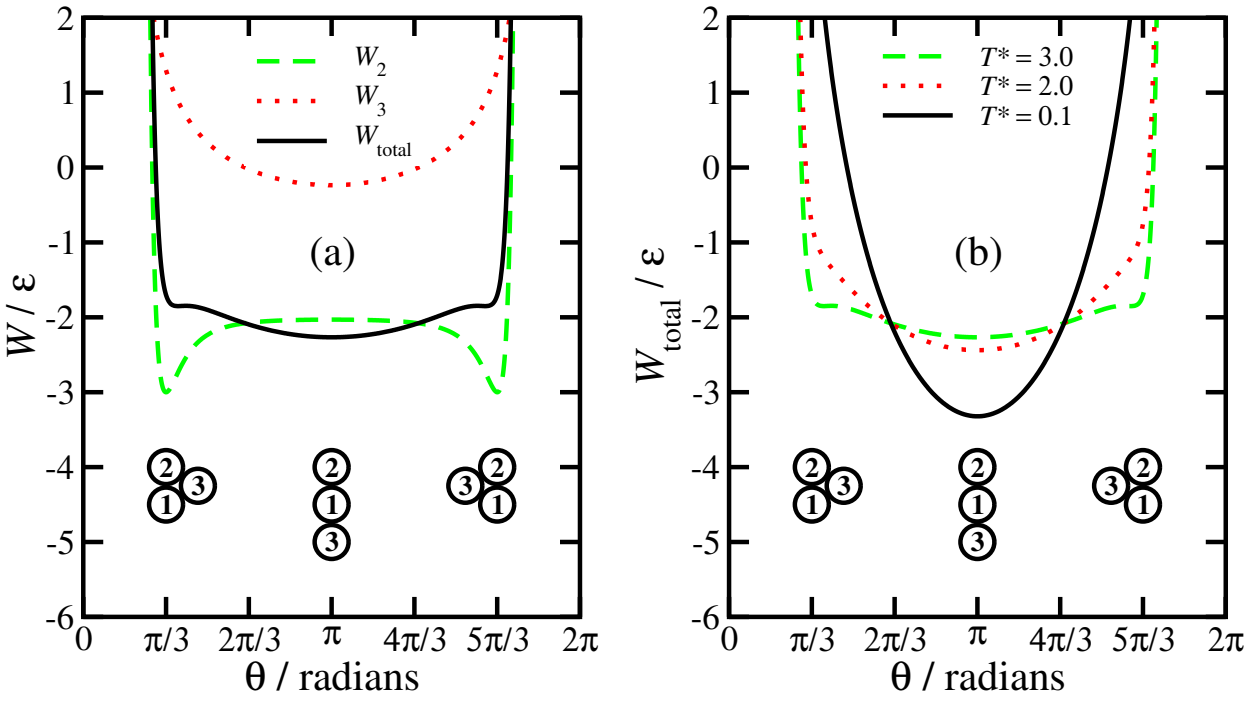

FIG. 2. Effective dipolar coupling constant λ_{eff} of the DSS fluid as a function of λ, using the Barker-Henderson route [Eq. (16)] (black solid line) and a minimum-energy criterion [Eq. (19)] (red dashed line).

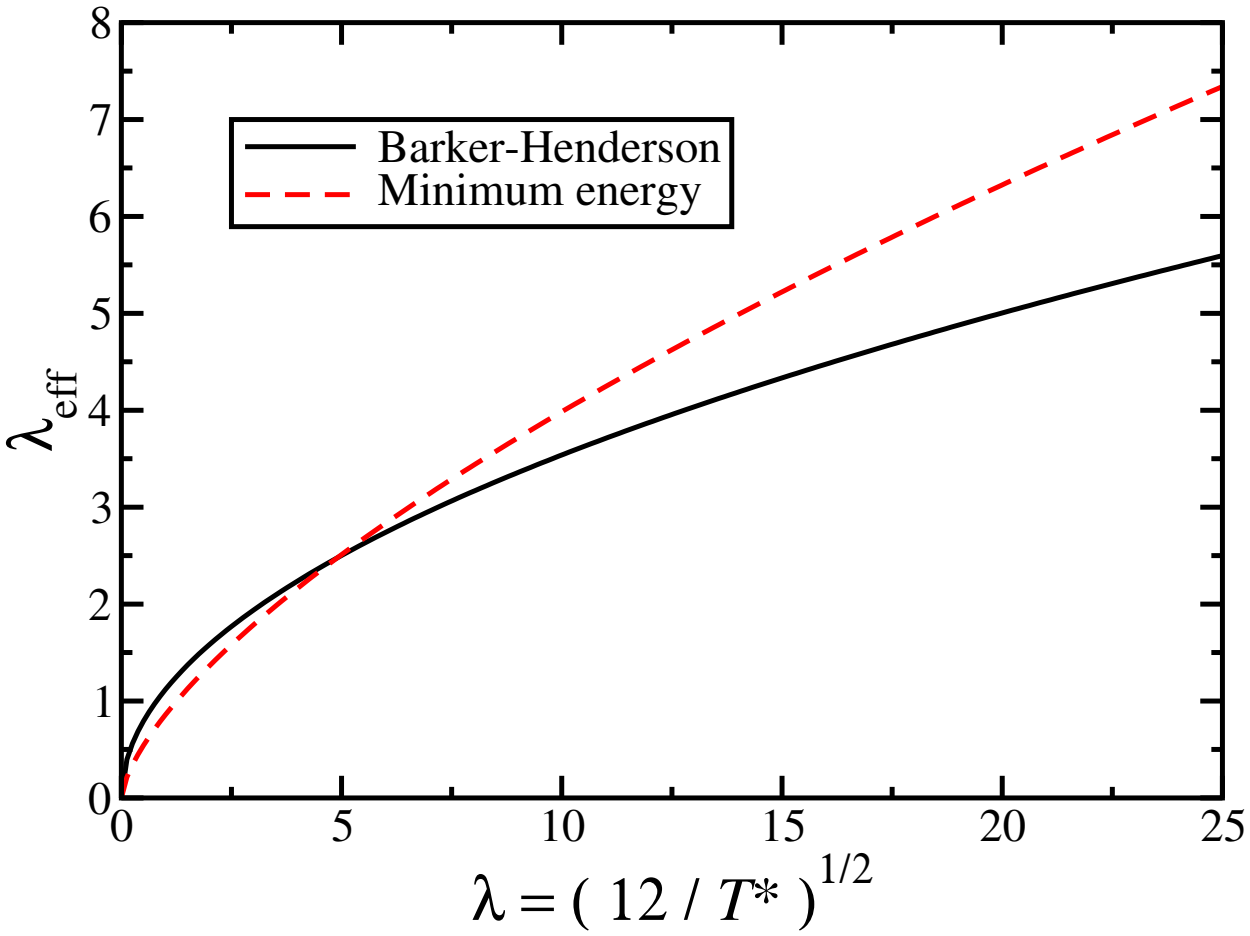

FIG. 3. Simulation snapshots of the DSS fluid (top row) and EMB fluid (bottom row) at $\rho^* = 0.007$ and with $\lambda = 1$, 2, 5, 10, and 20. Particles are shown with diameters equal to σ.

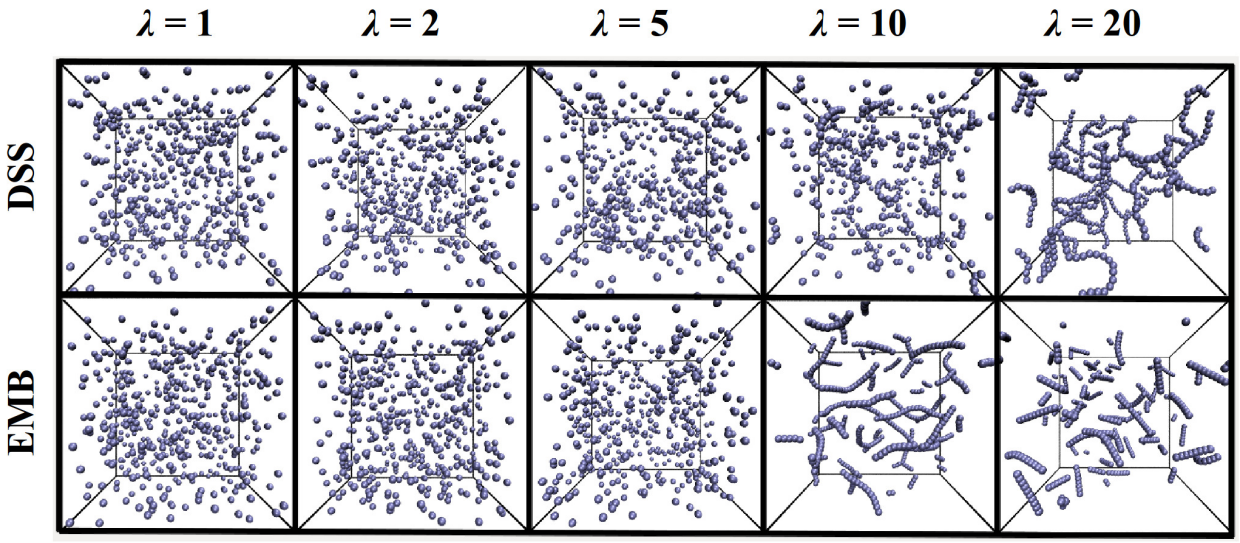

FIG. 4. Radial distribution functions $g(r)$ for DSS fluids (black solid lines) and EMB fluids (red dashed lines) with (from left to right) $\lambda = 1$, 2, 5, 10, 20, and (from top to bottom) $\rho^* = 0.007$, 0.100, 0.450.

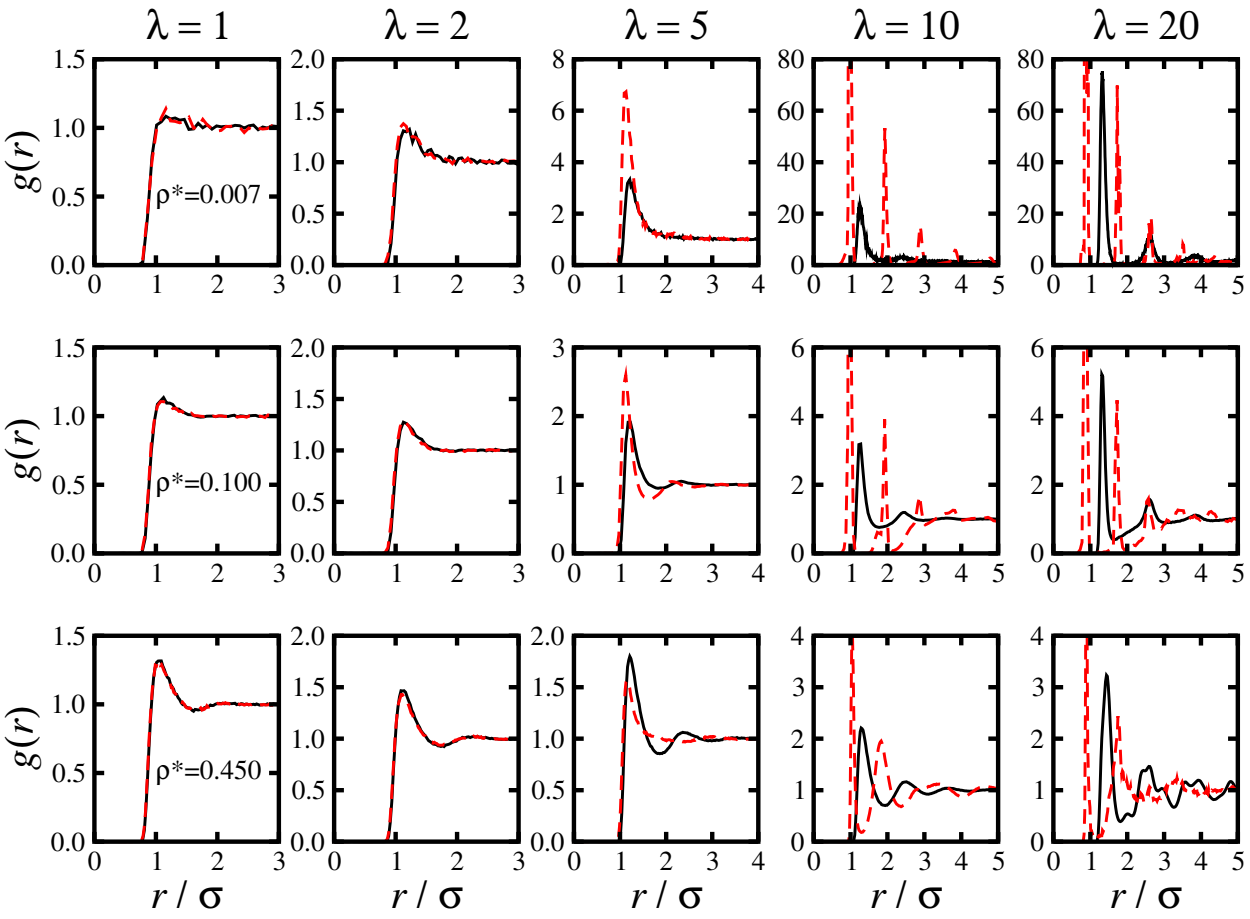

FIG. 5. Static structure factors $S(k)$ for DSS fluids (black solid lines) and EMB fluids (red dashed lines) with (from left to right) $\lambda = 1$, 2, 5, 10, 20, and (from top to bottom) $\rho^* = 0.007$, 0.100, 0.450.

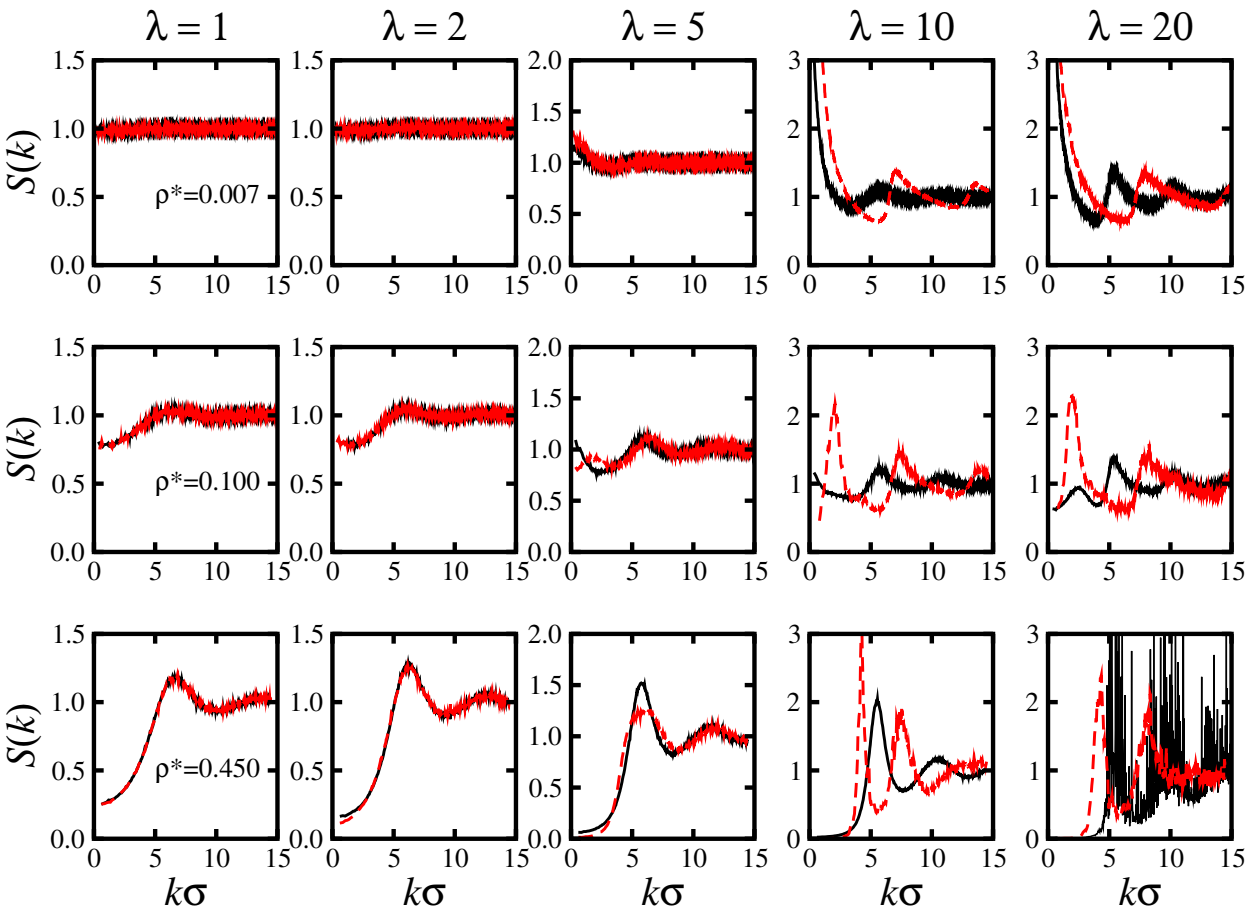

FIG. 6. Configurational parts of the internal energy E for the DSS and EMB systems at $\rho^* = 0.007$, plotted as functions of reciprocal reduced temperature $\beta^* = 1/T^*$. For the DSS system only: the soft-sphere (SS) and dipolar (D) contributions to the internal energy are shown; the solid lines are theoretical estimates valid at low temperatures – see Eqs. (26), (27), and (28), and the accompanying text; and the black dashed line is a fit to the DSS internal energy using a [2/2] Padé approximant in β^*.

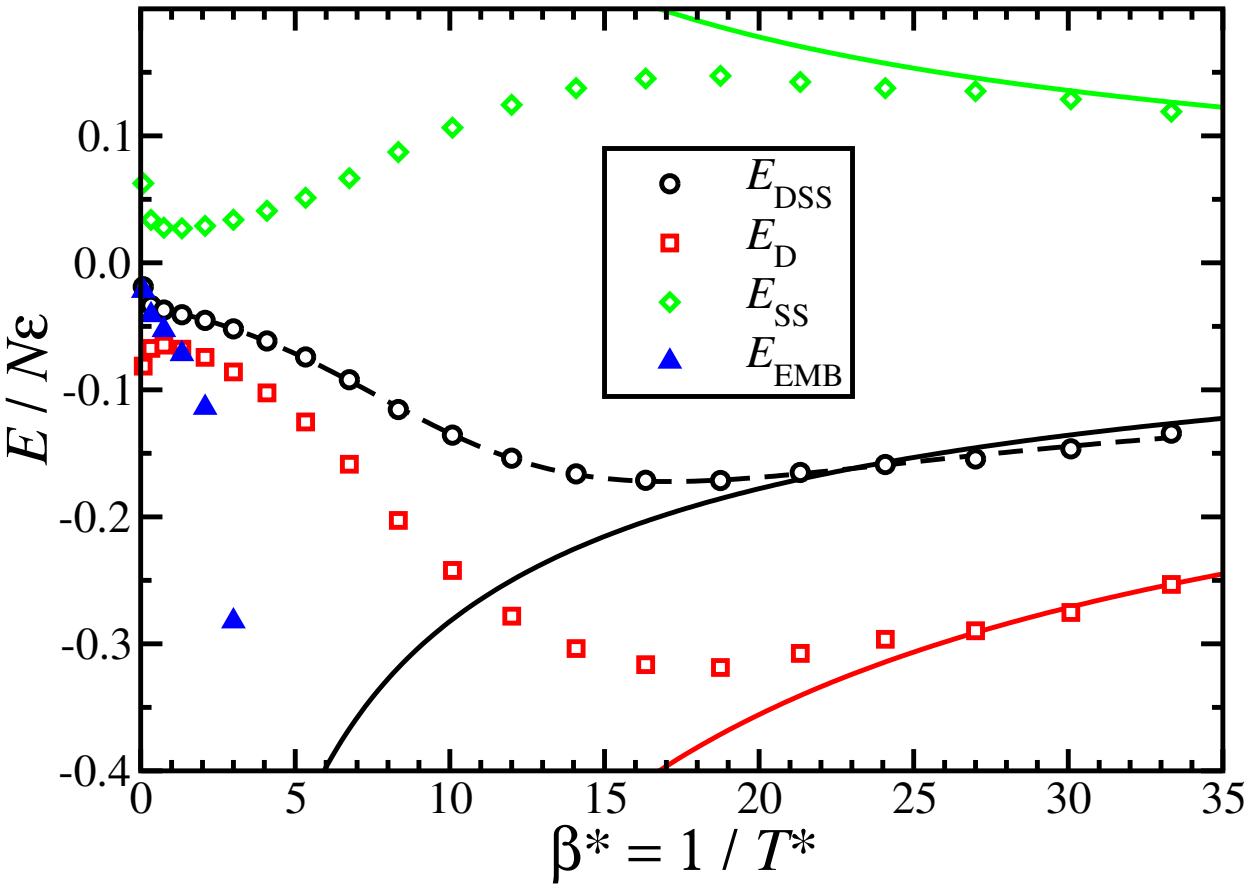

FIG. 7. Radial distribution functions $g(r)$ and static structure factors $S(k)$ for DSS and EMB (original and matched) fluids with $\lambda = 15$: (a)–(c) $\rho^* = 0.007$; (d)–(f) $\rho^* = 0.100$. The plots of $S(k)$ are on linear scales in (b) and (e), and on logarithmic scales in (c) and (f). The blue dot-dashed line in (c) is $(k\sigma)^{-1}$.

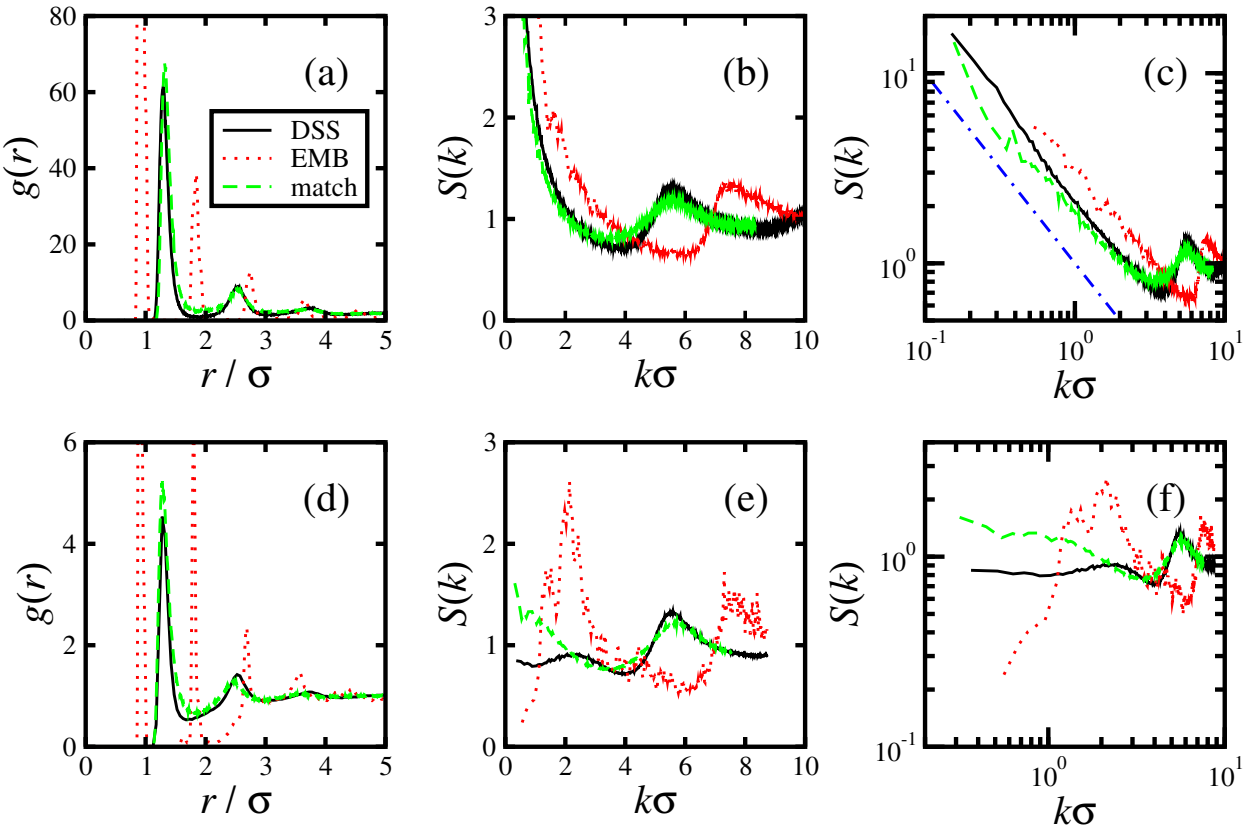

FIG. 8. Simulation snapshots of the DSS fluid (left column), original EMB fluid (middle column), and matched EMB fluid (right column) with $\lambda = 15$, and at $\rho^* = 0.007$ (first row) and $\rho^* = 0.100$ (bottom row). Particles are shown with diameters equal to σ.

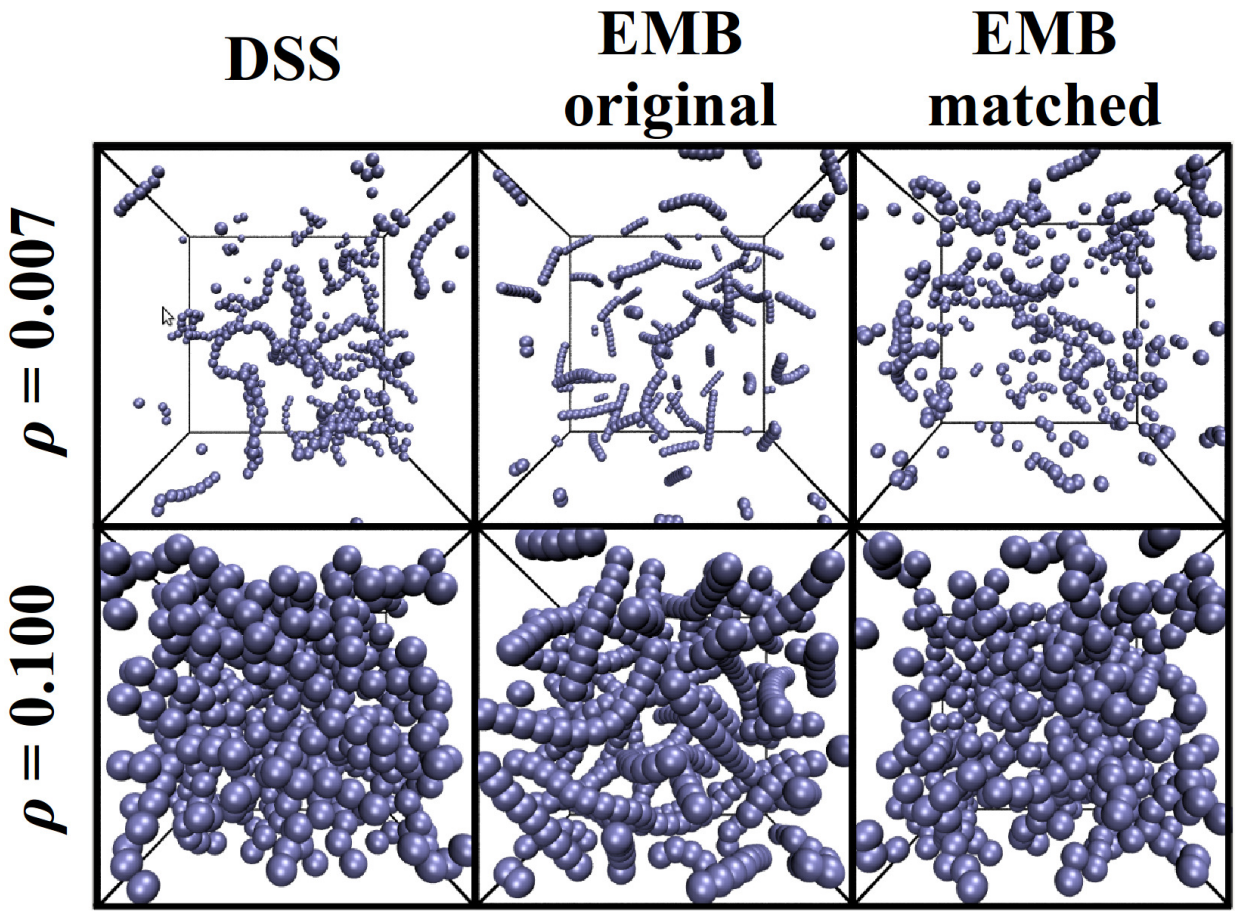

FIG. 9. (a) Vapor-liquid coexistence envelopes for EMB systems with various values of the AT interaction parameter a. (b) Critical parameters (T_c^*, ρ_c^*) plotted as functions of $a^{3/2}$: the linear regressions cross the abscissa at $a^{3/2} = 1.52(4)$ (T_c^*) and $a^{3/2} = 1.66(2)$ (ρ_c^*).

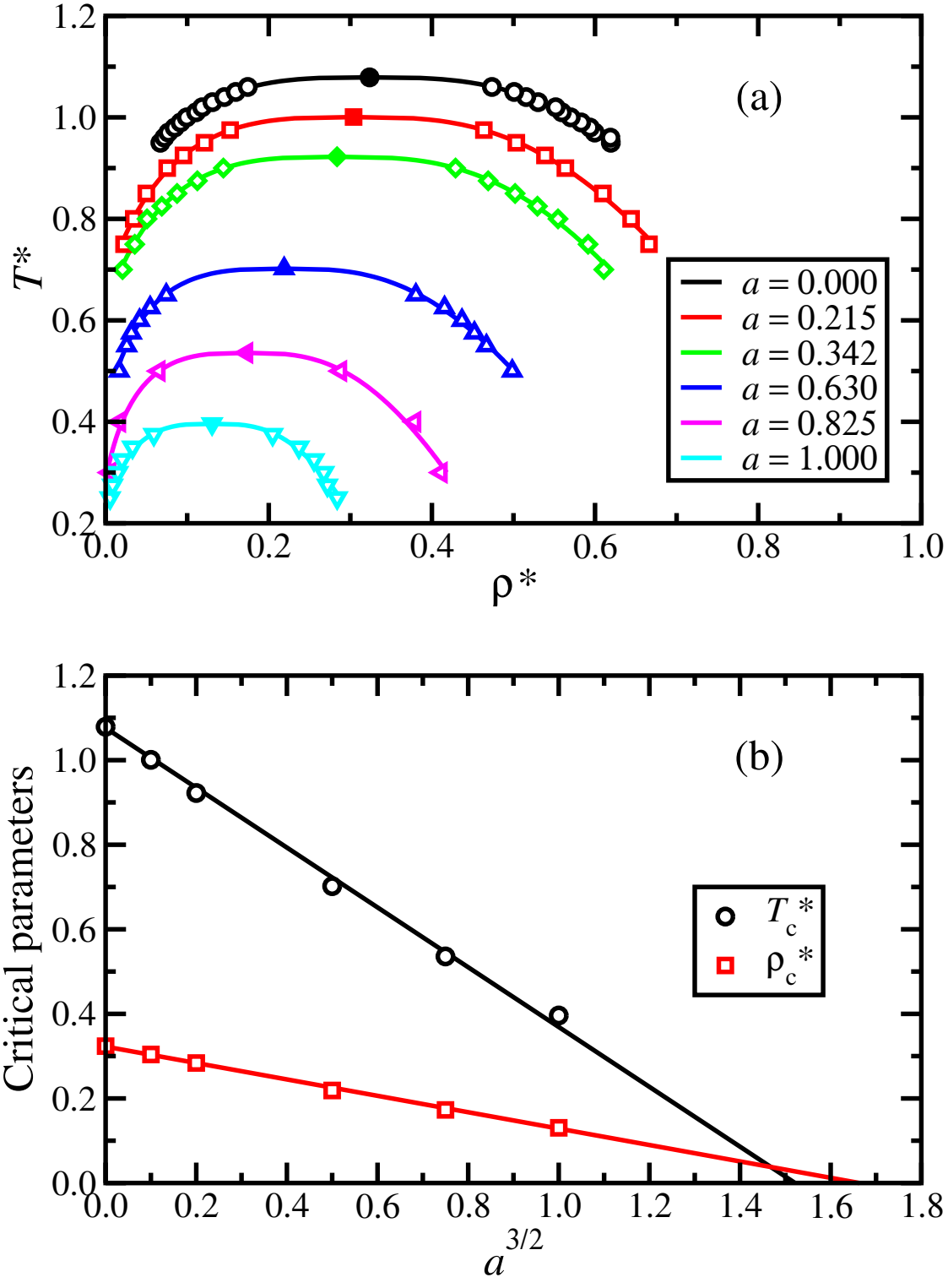

FIG. 10. Simulation snapshots of coexisting vapor and liquid phases in the EMB system: $a = 0.0$, $T^* = 0.95$ $(0.88T_c^*)$, $\rho^* = 0.067$ (vapor), $\rho^* = 0.62$ (liquid); $a = 1.0$, $T^* = 0.25$ $(0.63T_c^*)$, $\rho^* = 0.0055$ (vapor), $\rho^* = 0.28$ (liquid). Particles are shown with diameters equal to σ.

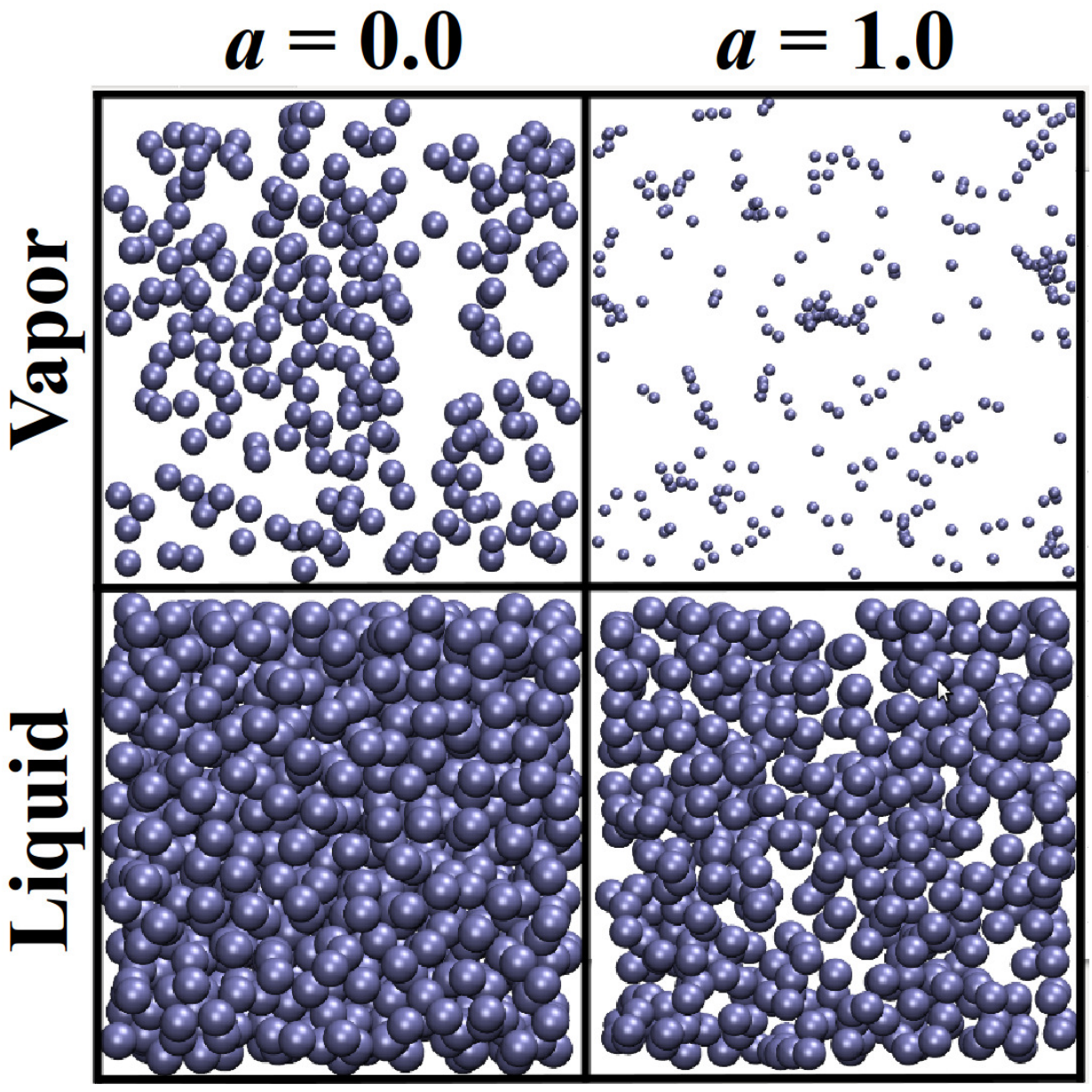

FIG. 11. Radial distribution functions $g(r)$ of the coexisting vapor and liquid phases in the EMB system: (a) the vapor phases with $a = 0.0$ ($T^* = 0.95$, $\rho^* = 0.067$) and $a = 1.0$ ($T^* = 0.25$, $\rho^* = 0.0055$); (b) the liquid phases with $a = 0.0$ ($T^* = 0.95$, $\rho^* = 0.62$) and $a = 1.0$ ($T^* = 0.25$, $\rho^* = 0.28$).